RSC Advances

PAPER

View Article Online
View Journal | View Issue

Cite this: *RSC Adv.*, 2023, **13**, 27203

Facile synthesis of Ag/ZIF-8@ZIF-67 as an electrochemical sensing platform for sensitive detection of halonitrophenols in drinking water†

Jiaxin Xiao,[ab] Shumin Zhu, *[ab] Lingjun Bu,[ab] Yuan Chen,[ab] Ruoxi Wu [ab] and Shiqing Zhou[ab]

Halonitrophenols (HNPs) are an emerging type of aromatic disinfection byproduct, with detected concentrations of ~nmol L^{-1} in source water and drinking water. Currently, there are no standard methods for identifying HNPs, and most of the reported methods are time-consuming and equipment-dependent. A core–shell metal–organic framework (MOF) based electrochemical sensor (Ag/ZIF-8@ZIF-67) capable of detecting 2,6-dichloro-4-nitrophenol (2,6-DCNP) is reported in this study. The electrochemical sensor obtains the concentration of 2,6-DCNP by detecting the peak current passing through the sensor. In this sensor, Ag nanoparticles (AgNPs) play a key role in electrochemical sensing by reducing nitro groups *via* electron transfer, and porous structure with a large surface area is offered by ZIF-8@ZIF-67. The cyclic voltammetry (CV) response of Ag/ZIF-8@ZIF-67 was found to be approximately 1.75 times and 2.23 times greater than that of Ag/ZIF-8 and Ag/ZIF-67, respectively, suggesting an ideal synergistic effect of the core–shell structures. The Ag/ZIF-8@ZIF-67 sensor exhibited exceptional sensitivity to 2,6-DCNP, exhibiting a broad linear response range (R^2 = 0.992) from 240 nmol L^{-1} to 288 μmol L^{-1} and a low detection limit of 20 nmol L^{-1}. Furthermore, the sensor exhibited good anti-interference for isomers and common distractors in water, excellent stability and reproducibility, and high recovery in actual water samples. Our reported sensor gives a novel strategy for sensitive, selective, and *in situ* detection of 2,6-DCNP in practical analysis.

Received 15th June 2023
Accepted 28th August 2023

DOI: 10.1039/d3ra04039a

rsc.li/rsc-advances

1. Introduction

Disinfection byproducts (DBPs) of structural diversity appeared in the public view after the first detection of chloroform in drinking water in the 1970s.[1,2] Since then, the carcinogenicity and cytotoxicity of DBPs have been gradually revealed, and the occurrence of many diseases has been thought to be associated with exposure to DBPs.[3–8] To date, trihalomethanes (THMs) and haloacetic acids (HAAs) have been regulated in many countries/areas,[9–11] and corresponding standard analytical methods have been well developed, with satisfactory accuracy and selectivity. However, more and more unregulated DBPs are frequently being detected in drinking water,[12,13] generally with more complex structures and higher toxicity, among which aromatic DBPs have attracted much attention in recent years.[14–16] Although the concentrations of aromatic DBPs are relatively low (~nmol L^{-1}) in drinking water,[17,18] it should be noted that they account for a large proportion of cytotoxicity resulting from the total organic halogens,[19] we compared the cytotoxicity of several common aromatic DBPs, and found that halonitrophenols (HNPs) showed the highest cytotoxicity.

There are some studies focusing on the occurrence and formation mechanisms of HNPs in the last decades,[9,20] but the convenient analysis of trace HNPs remains a bottleneck. Currently, high-performance liquid chromatography (HPLC) tandem mass spectrometry (MS) is the most-frequently used instrument to determine HNPs of nmol L^{-1} to μmol L^{-1}.[12,21] In spite of the high accuracy, selectivity, and sensitivity of HPLC/MS, the analysis process is complex and laborious, ultimately requiring expensive instruments and elaborate preprocessing.[22,23] Therefore, development of novel methods for accurate, *in situ*, and rapid determination of HNPs is necessary. Electrochemical sensing techniques and electrochemical biosensing approaches could effectively detect various substances,[24–26] including DBPs,[27,28] such as trichloroacetic acid (TCAA),[29] which thereby have much potential for determining HNPs. Electrochemical sensors could enable the real-time and *in situ* analysis of HNPs in drinking water using the appropriate electrodes. Herein, we choose 2,6-dichloro-4-nitrophenol (2,6-DCNP) as the model compound

[a]*Hunan Engineering Research Center of Water Security Technology and Application, College of Civil Engineering, Hunan University, Changsha 410082, PR China. E-mail: zshuminwater@163.com; Tel: +86 731 88821441*

[b]*Key Laboratory of Building Safety and Energy Efficiency, Ministry of Education, Hunan University, Changsha 410082, PR China*

† Electronic supplementary information (ESI) available. See DOI: https://doi.org/10.1039/d3ra04039a

for electrochemical sensing. The dechlorination reactions are usually used to show current signals in TCAA sensing,[30,31] while for 2,6-DCNP, the reduction of the nitro-moiety is occurs more readily in the electrochemical process, which however could be affected by the dechlorination reactions,[32] making the quantitative detection of 2,6-DCNP difficult. Also, unmodified electrodes are tardy for electron transport in electrochemical sensors.[33] Thus, how to prepare an electrochemical sensor with high sensitivity and selectivity is an issue to be resolved.

In recent decades, several strategies were proposed to amplify the current signals, including preparing materials of high electro-catalytic ability, etching more reaction sites, or cascading sensor array,[34,35] the first of which is the most investigated one. For example, researchers tried to employ metal oxides as electrode materials to detect nitrophenols, delivering a sensor limit of detection (LOD) of ~1 μmol L^{-1}.[32,36–38] With the introducing of carbon-based materials into metal oxides, the LOD was reduced to ~0.1 μmol L^{-1}.[39] Despite significant improvements in sensitivity through surface modification, requirements for detecting 2,6-DCNP in real drinking water cannot be met. Quite recently, successful application of metal–organic frameworks (MOFs) offered alternative methods to decrease the LOD for electrochemical sensing 2,6-DCNP, MOFs have gained increasing prominence in the field of electrochemical sensing due to their unique attributes of high surface area, facile synthesis, and tunable properties of metals, ligands, and porosity. These distinctive characteristics bestow MOFs with advantages not inherent in other materials.[40–43] Further, the confined synthesis process could lead to the formation of core–shell structures due to the continued growth of MOFs on the surface,[44,45] which show properties of both core and shell materials. When loading noble metal nanoparticles (*e.g.*, Ag) on the surface of core–shell materials, not only can the nanoparticles be well dispersed, but the catalytic performance can be improved. According to previous research,[46–49] AgNPs have demonstrated high catalytic activity, while the carrier ZIF-8@ZIF-67 possesses a high specific surface area and provides abundant oxygen vacancies. The coupling of AgNPs with ZIF-8@ZIF-67 effectively combines the advantages of both, this is also the reason for loading AgNPs onto the MOFs. To the best of our knowledge, there is no study focusing on electrochemical sensors of 2,6-DCNP using the core–shell MOFs.

In this study, we present an electrochemical sensor (Ag/ZIF-8@ZIF-67) with high sensitivity for detecting 2,6-DCNP (Scheme 1). Herein, ZIF-8@ZIF-67 was chosen to be a framework material for loading AgNPs, which effectively addressed the drawback of nanoparticle aggregation. Simultaneously, AgNPs provided excellent conductivity and catalytic activity to the MOFs. The microstructure, electrochemical mechanism, and sensing performance towards 2,6-DCNP of the prepared Ag/ZIF-8@ZIF-67 were investigated. As an electrochemical sensing platform, Ag/ZIF-8@ZIF-67 exhibited excellent conductivity, selectivity, and sensitive sensing performance, holding tremendous application potential in the field of drinking water sensing.

2. Experimental section

2.1. Chemicals

Sinopharm Chemical Reagent Co, Ltd provided $Zn(NO)_3 \cdot 6H_2O$, $Co(NO)_3 \cdot 6H_2O$, $AgNO_3$, and methanol (C_2H_5OH). Aladdin Chemistry Co. supplied 2-methylimidazole (2-Meim), and *N*-hexane was purchased from Macklin Biochemical Co. Sigma-Aldrich Co. provided polyvinylpyrrolidone (PVP). All chemicals used in this study were of analytical reagent grade and did not require any further purification.

2.2. Characterization

To examine the surface morphology and structure of Ag/ZIF-8@ZIF-67, we conducted scanning electron microscopy (SEM) and high-resolution transmission electron microscopy (HRTEM) using Tescan Mira-3 (Czechia) and FEI Talos (USA), respectively. Additionally, the crystalline phase was analyzed by X-ray diffraction (XRD) using a Bruker D8. We determined the chemical state of Ag/ZIF-8@ZIF-67 using X-ray photoelectron spectroscopy (XPS) with an Axis Ultra DLD Kratos AXIS SUPRA instrument (USA). The specific surface area of Ag/ZIF-8@ZIF-67 was estimated by Barrett–Emmett–Teller (BET) theory. Electrochemical measurements were carried out using a three-electrode system consisting of a glassy carbon working electrode (3 mm diameter), a platinum sheet counter electrode, and a saturated-potassium-chloride silver chloride electrode (SSCE) reference electrode. The electrochemical workstation used for the measurements was a CHI 660E model from Shanghai, China.

2.3. Preparation of ZIF-8@ZIF-67

An optimized conventional method was employed to synthesize ZIF-8@ZIF-67.[50] As shown in Fig. S1,† specifically, 3.969 g of $Zn(NO)_3 \cdot 6H_2O$ and 4.106 g of 2-Meim were dissolved in 100 mL of methanol separately. Two solutions were mixed and stirred continuously for 36 h. The obtained white precipitate was collected by centrifugation, washed with methanol three times, and dried at 50 °C overnight to obtain white ZIF-8 powder.

The preparation of ZIF-8@ZIF-67 involved dispersing 0.25 g of ZIF-8 powder in 50 mL of methanol by sonication for 30 min. Next, 2.91 g of $Co(NO)_3 \cdot 6H_2O$ and 3.08 g of 2-Meim were added separately to 50 mL of methanol and stirred until the solutions became clear. The three solutions were then mixed and continuously stirred for 36 hours. The resulting purple precipitate was collected by centrifugation, washed three times with methanol, and dried at 50 °C overnight to obtain purple ZIF-8@ZIF-67 powder.

2.4. Preparation of Ag/ZIF-8@ZIF-67

According to the past research,[51,52] Ag was loaded onto the ZIF-8@ZIF-67 by dual solvent methods. ZIF-8@ZIF-67 of 0.1 g was dispersed in 20 mL of anhydrous *n*-hexane *via* sonication for 30 minutes. $AgNO_3$ (3.14 mg) was added to the above mixture and stirred for 3 hours. The product was collected by removing the supernatant and subsequently dried at 50 °C overnight. The Ag/

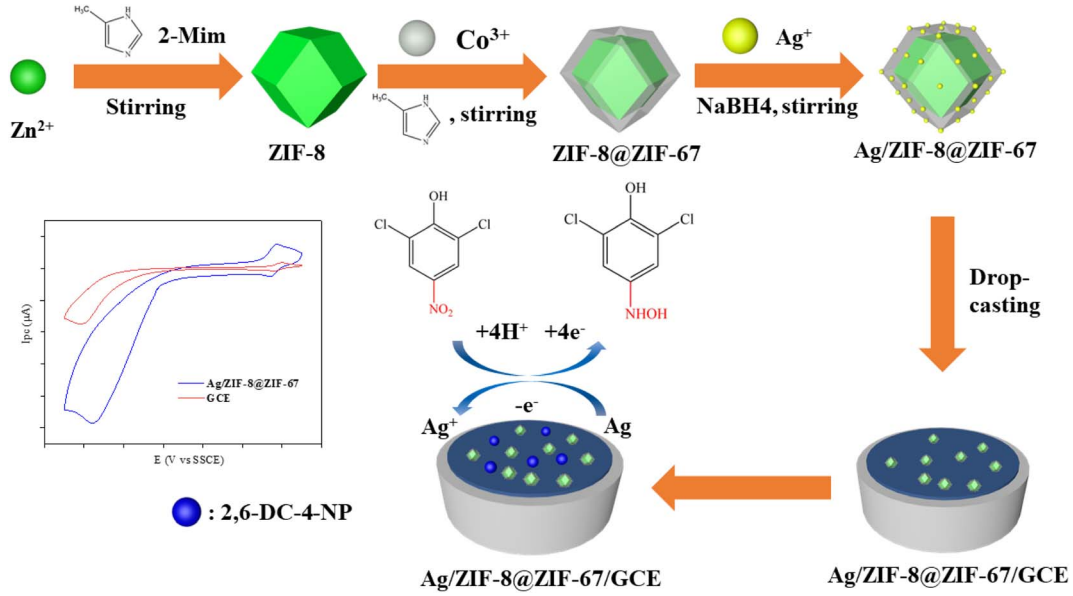

Scheme 1 Schematic illustration of the preparation and application of Ag/ZIF-8@ZIF-67/GCE.

ZIF-8@ZIF-67 powder was then treated with a freshly prepared $NaBH_4$ methanol solution (5 mL), stirred in the dark for 30 minutes. The product was washed with methanol thrice. Finally, the powder was dried under vacuum at 50 °C overnight. Similar steps were followed to synthesize Ag/ZIF-8 and Ag/ZIF-67.

2.5. Fabrication of the modified electrode

A bare glassy carbon electrode (GCE) was polished to a mirror surface with 1 μm, 0.5 μm, and 0.3 μm alumina powder on chamois leather. The GCE was then sonicated using ultrapure water for 10 min and dried in an oven until completely dry. After dispersing 2 mg Ag/ZIF-8@ZIF-67 in 1 mL ultrapure water, the mixture was sonicated for 30 minutes to produce a homogeneous suspension solution. 7 μL suspension was dropped onto the surface of GCE and dried to obtain the modified electrode. The modified electrodes, Ag/ZIF-8/GCE, Ag/ZIF-67/GCE, and AgNPs/GCE, were all prepared by the same methods as described above. The process for the preparation and application of Ag/ZIF-8@ZIF-67/GCE are detailed in ESI Text S1.†

2.6. Real water sample test

Tap water and swimming pool water (collected from Hunan University, Changsha, China) were used as the real water samples. To eliminate solid impurities, prior to analysis, each water sample was filtered through a 0.22 μm membrane. The filtered sample was then adjusted to a pH of 6.0 using phosphate-buffered solution before testing for the initial concentration of 2,6-DCNP using the electrochemical method. Subsequently, various amounts of standard solutions were added to the real water samples, and the 2,6-DCNP concentration was measured on an Ag/ZIF-8@ZIF-67/GCE using differential pulse voltammetry (DPV) technique.

3. Results and discussion

3.1. Characterizations of Ag/ZIF-8@ZIF-67

The microscopic morphology and structures of the prepared Ag/ZIF-8@ZIF-67 were analyzed using SEM and HRTEM. As shown in Fig. 1a and b, Ag/ZIF-8@ZIF-67 was a uniform rhombic dodecahedron with relatively smooth surface. Ag/ZIF-8@ZIF-67 has an average particle size of 450 nm (Fig. 1a), with a specific surface area of 425.26 $m^2\ g^{-1}$ (Fig. S2†), and the size of decorated AgNPs was determined to be approximately 15 nm (Fig. 1c). Several impurities were observed in the SEM images, some of which were formed due to the agglomeration of AgNPs, while others may be formed in the synthesis process for ZIF-67 particles. Besides, ZIF-8@ZIF-67 acting as the carrier remained its original morphology after nanoparticle loading.[53] As shown, AgNPs were bound to the carrier as spherical nanoparticles under the reduction of $NaBH_4$. A small portion of AgNPs was observed on the surface, which may be attributed to that most AgNPs were loaded in the pores of the ZIF-8@ZIF-67. Compared with previous studies,[54,55] the morphology of ZIF-8@ZIF-67 was similar to those of individual ZIF-8 or ZIF-67, due to the similar cell parameters and topology of both ZIF-8 and ZIF-67. Further, as depicted in Fig. 1d, successful reduction of Ag^+ can be observed through the obvious lattice stripe of AgNPs on the surface of ZIF-8@ZIF-67. The lattice spacing has the *d* value of 2.39 Å, corresponding to the (111) crystal plane of zero-valent Ag. Thus, according to the SEM and HRTEM images in Fig. 1, successful synthesis of Ag/ZIF-8@ZIF-67 could be confirmed.

Fig. 2a displays the XRD results of our prepared Ag/ZIF-8@ZIF-67, showing that the composites have a crystal structure similar to that of ZIF-8@ZIF-67. Of note, the position of the diffraction peaks in the XRD of Ag/ZIF-8@ZIF-67, the simulated XRD of ZIF-8@ZIF-67 (ESI Text S2†), and the XRD of ZIF-8 and ZIF-67 were highly consistent. Therefore, it can be concluded

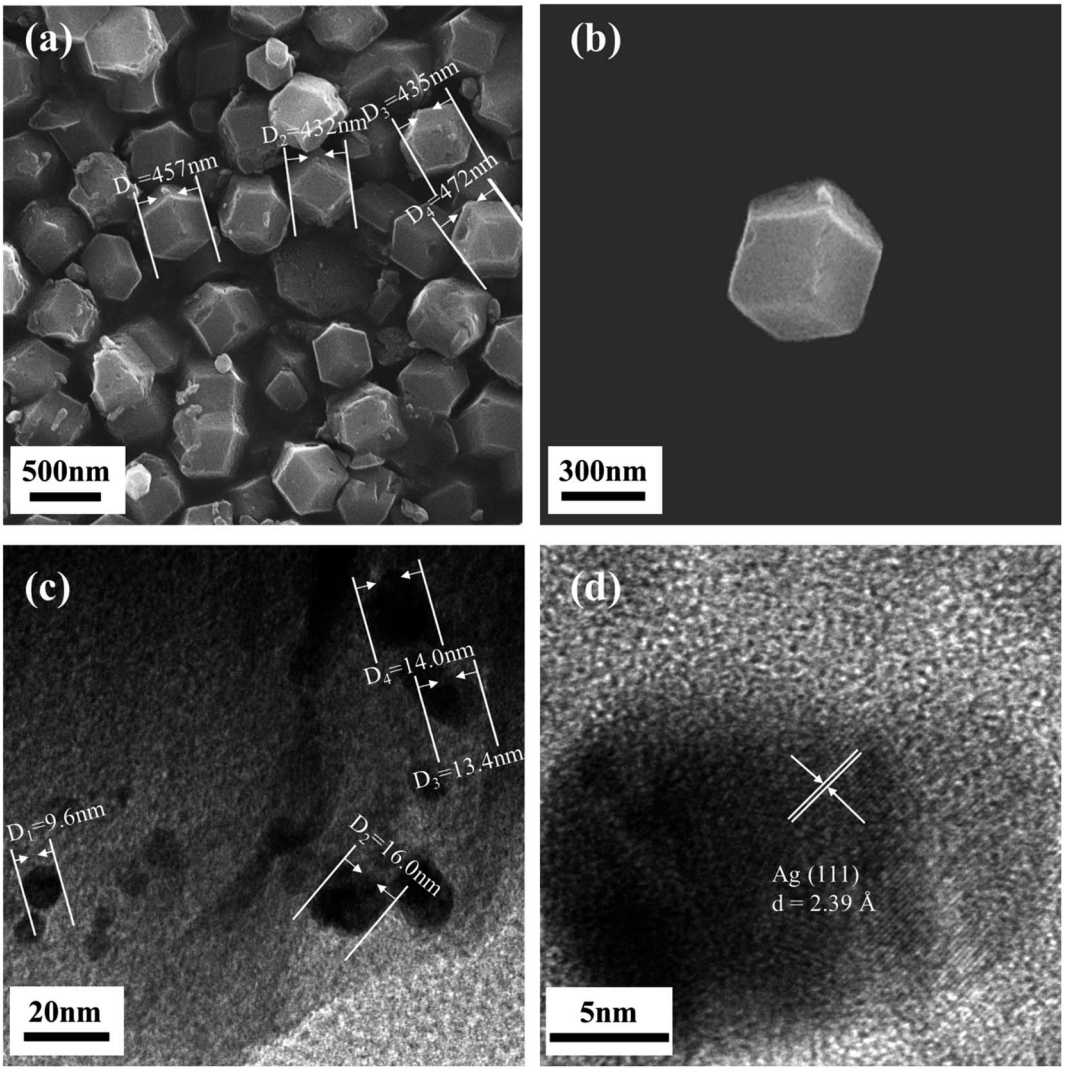

Fig. 1 SEM images of Ag/ZIF-8@ZIF-67 (a and b) and TEM images of Ag/ZIF-8@ZIF-67 (c and d).

that the synthesis of pure ZIF-8@ZIF-67 was successful and that the incorporation of AgNPs did not significantly affect the structure of ZIF-8@ZIF-67.[54,56,57] Compared to the individual ZIF-8 and ZIF-67, there are some additional diffraction peaks of Ag/ZIF-8@ZIF-67 at $2\theta = 24.4°$, 26.6°, and 29.6°, which correspond to (233), (134), (044) crystal facets, respectively, which are caused by the core–shell structure.

Further, the chemical composition, valence state, and elemental content of materials are determined by XPS (Fig. 2b–f). As shown in Fig. 2b, the full-spectrum scanning of XPS revealed the presence of Ag was 2.89%, which was 3% before preparation, demonstrating that there was no significant loss during the loading process. The C1s XPS spectrum was displayed in Fig. 2c. C1s was decoupled using fitting to obtain three characteristic peaks of C–C, C–N, and C–O. The relatively small area of the C–O peak in the obtained spectra indicated that damages to the structure of 2-Meim were controlled to the minimal in the synthesis process. In Fig. 2d, the two symmetric peaks were observed at 1021.8 and 1044.8 eV, corresponding to the binding energies of the Zn2p3/2 and Zn2p1/2 spin orbitals, respectively. This observation confirmed the presence of Zn^{2+} in the materials. Then, Fig. 2e displayed two peaks with binding energies of 781.3 eV and 797.2 eV, which corresponded to the Co2p3/2 and Co2p1/2 spin orbitals, respectively, thus indicating the presence of the Co^{2+} in the material. The peaks at binding energies of 368.3 eV and 374.3 eV, shown in Fig. 2f, corresponded to the Ag3d5/2 and Ag3d3/2 spin orbitals, respectively. These peaks indicated the presence of zero-valent Ag in the material. For further details on the crystal structure of ZIF-8@ZIF-67, refer to ESI Text S3.†

3.2. Electrochemical behavior of the sensor

The CV responses of bare GCE, Ag/ZIF-8, Ag/ZIF-67, and Ag/ZIF-8@ZIF-67 electrodes were tested. Upon the injection of 2,6-DCNP, noticeable redox peaks and high current response could be observed (Fig. 3a). As shown, three obvious redox peaks occurred at E values of −0.75 (R), 0.20 (O_1), and 0.19 V (R_1), of which O_1 and R_1 are couple of reversible redox peaks referring

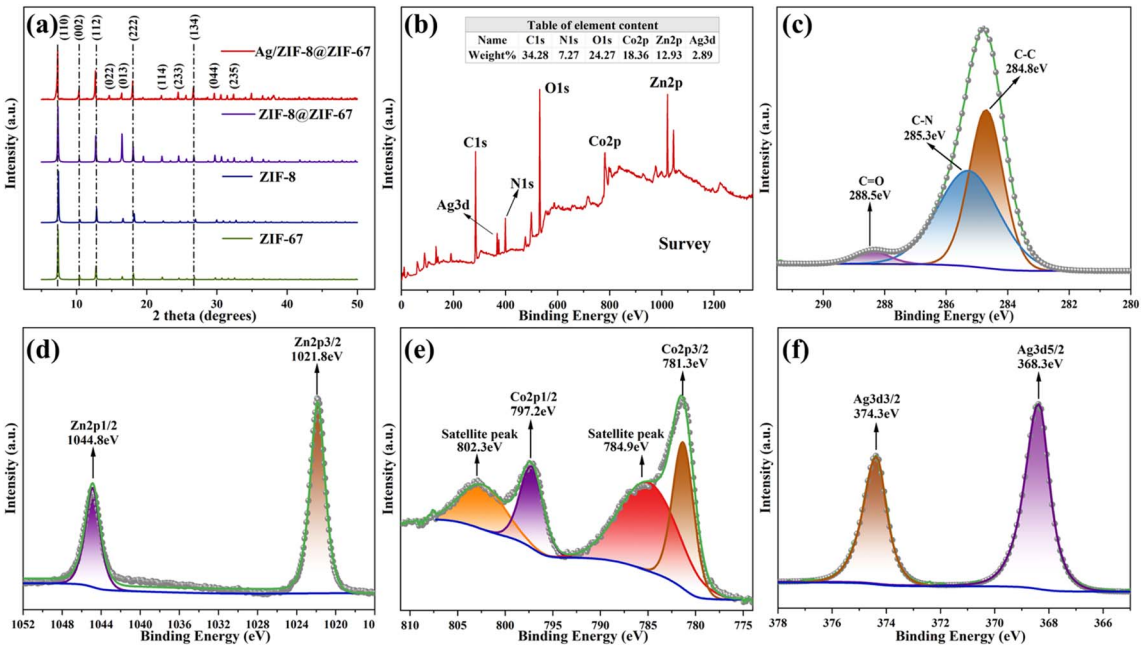

Fig. 2 XRD spectra of Ag/ZIF-8@ZIF-67, ZIF-8@ZIF-67, ZIF-8, and ZIF-67 (a) and XPS spectra of Ag/ZIF-8@ZIF-67 (b), XPS spectra of C1s (c); Zn2p (d); Co2p (e) and Ag3d (f) in Ag/ZIF-8@ZIF-67.

to an interconversion of 2,6-dichloro-4-hydroxylaminophenol and 2,6-dichloro-4-nitrosophenol. Also, reduction of 2,6-DCNP showed an intensely irreversible redox peak near $E = -0.75$ V,[58] which showed significantly larger signals when using Ag/ZIF-8@ZIF-67 electrode than the others. The CV results of Ag/ZIF-8@ZIF-67 electrode without 2,6-DCNP in solution were shown in Fig. S3,† which demonstrated the distinct reduction peak observed around −0.75 V was attributed to 2,6-DCNP, rather than the modification material itself. The electrochemical response for 2,6-DCNP on Ag/ZIF-8@ZIF-67 electrode was 1.75, 2.23, and 2.77 times higher than Ag/ZIF-8, Ag/ZIF-67, and bare GCE, respectively. The interaction between AgNPs and MOFs is also one of the reasons for the increase in peak current. Moreover, the noticeable increase in current signal on the modified electrode pointed towards the superior reduction performance of Ag/ZIF-8@ZIF-67, which accelerated the transformation of nitro-moiety to hydroxylamine, *via* expediting the electron transfer.

Electrochemical impedance spectroscopy (EIS) was then conducted, to further evaluate the charge transfer properties of the different electrodes. Charge-transfer resistance (R_{ct}) was determined by analyzing the diameter of the semicircle obtained from the fitted Nyquist plots, using the Randles equivalent circuit. As depicted in Fig. 3b, the order of R_{ct} values follows the order of Ag/ZIF-67 > Ag/ZIF-8 > Ag/ZIF-8@ZIF-67, which were in the opposite order of the reduction current signals. The relatively lower electron resistance observed in Ag/ZIF-8@ZIF-67 electrode can be attributed to the increased surface area of the

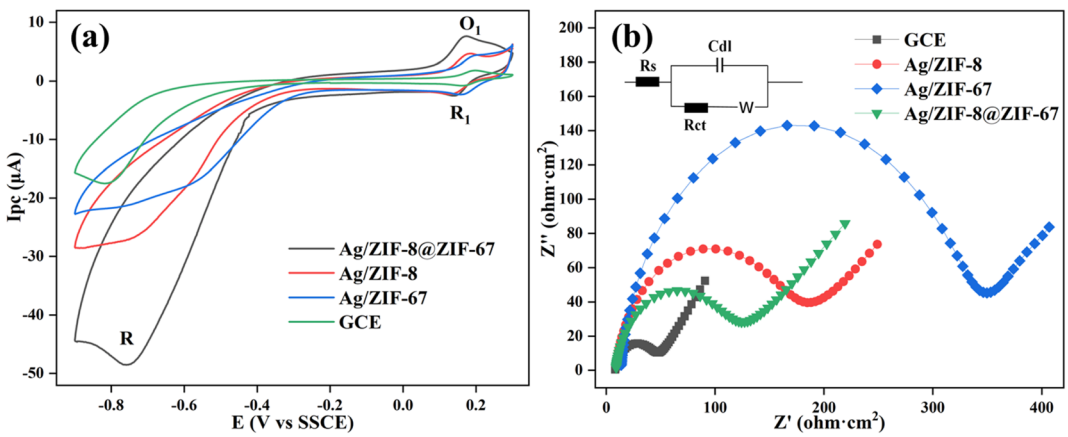

Fig. 3 CV responses of different electrodes in the presence of 20 mg per L 2,6-DCNP (a), EIS Nyquist plots of the electrodes in 0.1 mol per L KCl solution containing 5 mmol per L $[Fe(CN)_6]^{3-/4-}$ (1 : 1) (b); the frequency is from 0.01 to 100 000 Hz and the amplitude is 5 mV.

electrode and the improved dispersion of AgNPs. The rationale behind the selection of Ag/ZIF-8@ZIF-67 as the electrode modification material was attributed to the comparatively lower charge transfer resistance and higher specific surface area of Ag/ZIF-8@ZIF-67 in comparison to Ag/ZIF-8 and Ag/ZIF-67.

3.3. The optimization of experimental parameters

According to the discussions in section 3.2, the peak around −0.75 V was chosen as the typical peak of 2,6-DCNP, to linearly relate the peak current and 2,6-DCNP concentration.

As suspension volume and solution pH could significantly impact the potential and current peak, we investigated their effects to optimize the experimental parameters to further amplify the signals, using the DPV method. As shown in Fig. S4a,† the electrochemical response gradually increased and peaked at 7 μL when the volume of the suspension on GCE was increased from 4 to 7 μL. With the further increase in suspension volume to 8, 9, and 10 μL, the electrochemical response began to decrease, which may be resulted from the thicker layer of Ag/ZIF-8@ZIF-67, hindering electron transmission and reducing the available catalytic active sites. Consequently, the suspension volume of 7 μL was selected for subsequent experiments. With this volume, the mass concentration of Ag/ZIF-8@ZIF-67 on GCE was measured to be 1.98 μg mm^{-2}. As shown in Fig. S4b,† the optimal pH for the sensor was observed at 6, with the highest I_{pc} value. This was because that (1) AgNPs are unstable at acid conditions; and (2) electron density of the nitro-moiety increased at alkaline conditions, thereby slowing down the reduction of 2,6-DCNP.[32] Apart from I_{pc}, the E_{pc} values exhibited a linear relationship with increasing pH values, characterized by a decrease in value as follow:

$$E_{pc}\ (V) = -0.052\ pH - 0.219\ (R^2 = 0.997)$$

Using the Nernst formula ($E_{pc} = E - 0.059\ (m/n)$ pH, where m and n denote the number of protons and electrons.[59]), a slope of 0.052 was obtained for the linear equation. This value is nearly equivalent to 0.059, suggesting that the reaction involved an equal number of protons (m) and electrons (n).

3.4. Quantitative detection of 2,6-DCNP

Different concentrations (0–288 μmol L^{-1}) of 2,6-DCNP were tested under the optimal conditions for measurement. As shown in Fig. 4a, the current peak value at $E = -0.75$ V increased with the increase in 2,6-DCNP concentration. We plotted the relationship between the current (I_{pc}, μA) and 2,6-DCNP concentration (C, μmol L^{-1}) in Fig. 4b, of which the linear range was observed at 0.24–288 μmol L^{-1} ($R^2 = 0.992$). The corresponding LOD was determined as 0.02 μmol L^{-1} based on the signal-to-noise ratio (S/N = 3). Also, the sensitivity of Ag/ZIF-8@ZIF-67 when determining 2,6-DCNP was calculated as 0.58 μA $(\mu mol\ cm^2)^{-1}$, where sensitivity is defined as slope/area (slope refers to the slope of the fitting curve equation, and area refers to the area of Ag/ZIF-8@ZIF-67 on GCE). Previous studies have never addressed the electrochemical sensing of HNPs, and our study well fills this gap. Compared with other nitrophenols sensors,[36,60–63] our sensor exhibited better performance, and the synthesis process of Ag/ZIF-8@ZIF-67 was more environmentally friendly and practical since no additional operations like heating or sonication are required.

3.5. Selectivity, stability, and reproducibility of the sensor

To ensure the analytical performance of Ag/ZIF-8@ZIF-67 on 2,6-DCNP in complex detection environments, the modified electrode was required to have high anti-interference properties and reliable repeatability. To assess the selectivity of the sensor, the impact of typical interferents and analogs with similar structures on the 2,6-DCNP sensor signal was examined. In this study, the interferents (20 mg L^{-1}) chosen were Mg^{2+}, Cu^{2+}, Ca^{2+}, phenol, nitrobenzene (NB), *p*-nitrophenol (*p*-NP), 4-chloro-2-nitrophenol (4-Cl-2-NP), 2,4-dichloro-5-nitrophenol (2,4-DC-5-NP), and humus acid (HA). The effects of interfering substances on Ag/ZIF-8@ZIF-67 electrode's DPV response were shown in Fig. 5a and S5,† and the raw data was recorded in Table S1.† As shown in Fig. 5a, compared to other compounds, the Ag/ZIF-8@ZIF-67 sensor exhibited a notably greater response to 2,6-DCNP. For example, the sensor response of 2,6-DCNP was more than 12-fold higher than that of 2,4-DC-5-NP and more than 3-fold higher than that of *p*-NP. Despite the similar structure of interfering substances, the selectivity experiments revealed the remarkable selectivity of Ag/ZIF-8@ZIF-67 towards 2,6-DCNP. This high selectivity was attributed to the excellent selective catalysis by Ag/ZIF-8@ZIF-67 and the intrinsic advantage of electrochemical detection.

Besides selectivity, the reproducibility and stability are equally crucial parameters in evaluating the electrochemical sensors. As shown in Fig. 5b, the reproducibility of the modified electrode was evaluated by measuring 20 mg per L 2,6-DCNP five times using the same Ag/ZIF-8@ZIF-67/GCE. The relative standard deviation (RSD) of the current response was calculated as 3.14%. Further, the RSD was calculated as 5.15% when detecting the same concentration of 2,6-DCNP by five different modified electrodes. This indicated that the electrochemical sensor has strong reproducibility in the detection of 2,6-DCNP. The stability of electrode material is also a crucial factor that must be ensured to enhance the overall performance of our sensor. Fig. S6† exhibits that the electrode retained 95.09% of its initial current after being stored for seven days under environmental conditions, suggesting satisfactory stability of Ag/ZIF-8@ZIF-67. The decline in activity of AgNPs during storage might account for the reduction in current responsiveness.

3.6. Detection in real water samples

To evaluate the practicality of the electrochemical sensor, real water samples, namely tap water and swimming pool water, were chosen as the backgrounds. The DPV response revealed that 2,6-DCNP was not detected in the real water samples in Table S2,† therefore, different amounts of 2,6-DCNP were added into real water samples. The recoveries of 4.8 μmol per L and 48 μmol per L 2,6-DCNP were 98.41% and 101.64% for tap water samples, respectively, which were 98.24% and 100.96% in swimming pool water samples. The findings provided evidence

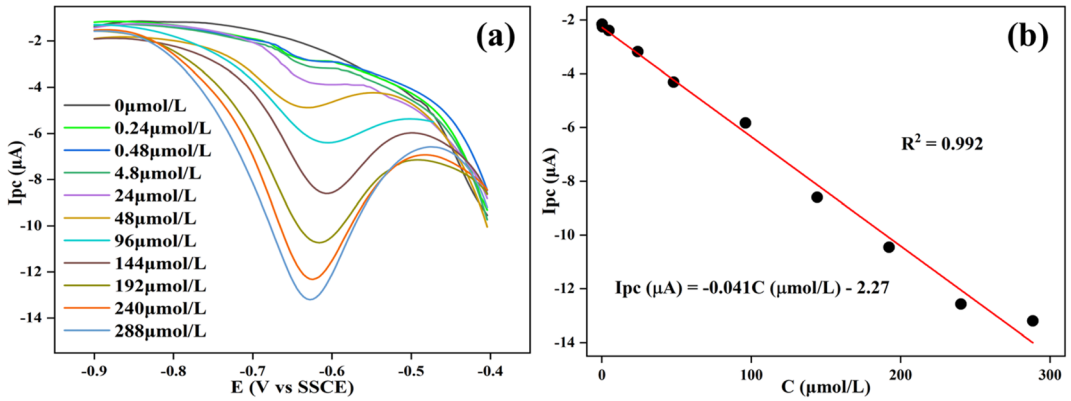

Fig. 4 DPV responses of the sensor to different concentration of 2,6-DCNP (0–288 μmol L^{-1}) in 0.1 mol per L PBS (pH = 6) (a). The linear relationship between I_{pc} and 2,6-DCNP concentration (b).

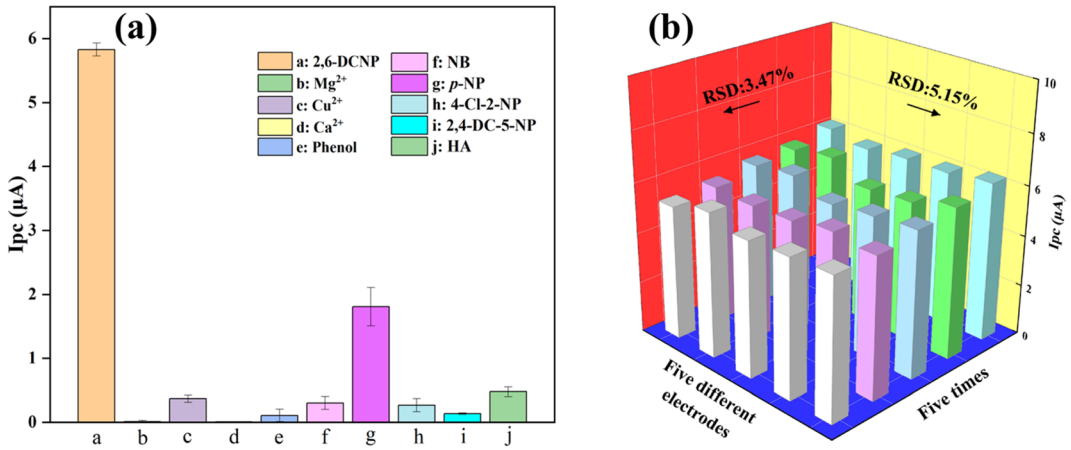

Fig. 5 Influence of interferents (2,6-DCNP, Mg^{2+}, Cu^{2+}, Ca^{2+}, phenol, NB, P-NP, 4-Cl-2-NP, 2,4-DC-5-NP, HA) on detection of 20 mg per L 2,6-DCNP (a). Error bars represent the standard deviation ($n = 3$), and sensor's responses were obtained by five different electrodes and one electrode test five times (b).

of the reliability and potential application of Ag/ZIF-8@ZIF-67 for detecting 2,6-DCNP in actual water samples, thus confirming the feasibility of using this electrochemical sensor in practical scenarios.

4. Conclusions

The present study reports the successful development of a specialized electrochemical sensor, namely Ag/ZIF-8@ZIF-67, with high sensitivity and selectivity for detecting 2,6-DCNP. The main conclusions can be summarized as follows:

(1) By utilizing the epitaxial growth and two-solvent methods, Ag/ZIF-8@ZIF-67 was synthesized as an electrode material. This facile synthesis approach allowed us to synergistically combine the high catalytic activity of AgNPs with the high specific surface area of core–shell MOF structures.

(2) The surface of the GCE was coated with a thin film of Ag/ZIF-8@ZIF-67, as evidenced by the SEM and HRTEM images, which demonstrated the uniform dispersion of AgNPs within the ZIF-8@ZIF-67 framework.

(3) Ag/ZIF-8@ZIF-67 was prepared and utilized to detect 2,6-DCNP, which showed remarkable performance compared to conventional detection techniques. The sensor displayed superior selectivity, an extended linear range of 0.24–288 μmol L^{-1}, and an impressively low detection limit of 20 nmol L^{-1} for detection of 2,6-DCNP.

(4) The sensor reported in this study performed well when detecting 2,6-DCNP in actual water samples such as drinking water or swimming pool water.

Conflicts of interest

There are no conflicts to declare.

Acknowledgements

This work was financially supported by the National Natural Science Foundation (52200014 and 52100007), and the Natural Science Foundation of Hunan Province (2021JJ40106).

References

1 G. Hua and D. A. Reckhow, *Water Res.*, 2007, **41**, 1667–1678.
2 J. Han, X. Zhang, J. Jiang and W. Li, *Environ. Sci. Technol.*, 2021, **55**, 5906–5916.
3 J. Jiang, J. Han and X. Zhang, *Environ. Sci. Technol.*, 2020, **54**, 1646–1656.
4 X. X. Wang, B. M. Liu, M. F. Lu, Y. P. Li, Y. Y. Jiang, M. X. Zhao, Z. X. Huang, Y. Pan, H. F. Miao and W. Q. Ruan, *J. Environ. Manage.*, 2021, **282**, 111951.
5 X. Yang, W. Ou, Y. Xi, J. Chen and H. Liu, *Environ. Sci. Technol.*, 2019, **53**, 7019–7028.
6 L. Yang, X. Chen, Q. She, G. Cao, Y. Liu, V. W. Chang and C. Y. Tang, *Environ. Int.*, 2018, **121**, 1039–1057.
7 X. F. Li and W. A. Mitch, *Environ. Sci. Technol.*, 2018, **52**, 1681–1689.
8 J. M. Allen, M. J. Plewa, E. D. Wagner, X. Wei, K. Bokenkamp, K. Hur, A. Jia, H. K. Liberatore, C. T. Lee, R. Shirkhani, S. W. Krasner and S. D. Richardson, *Environ. Sci. Technol.*, 2022, **56**, 392–402.
9 Y. Wu, X. Chen, L. Bu, S. Zhu, S. Zhou and W. Chu, *ACS ES&T Water*, 2022, **2**, 798–806.
10 C. Sfynia, T. Bond, R. Kanda and M. R. Templeton, *Chemosphere*, 2020, **248**, 125940.
11 J. Li, M. T. Aziz, C. O. Granger and S. D. Richardson, *Environ. Sci. Technol.*, 2021, **55**, 12994–13004.
12 S. Hu, H. Y. Kaw, L. Zhu and W. Wang, *Water Res.*, 2022, **219**, 118547.
13 A. A. Cuthbertson, H. K. Liberatore, S. Y. Kimura, J. M. Allen, A. V. Bensussan and S. D. Richardson, *Anal. Chem.*, 2020, **92**, 3058–3068.
14 K. Liu, M. Li, Z. Zhu, B. Gao, H. Zeng, Y. Ma and L. Fang, *Environ. Sci.: Water Res. Technol.*, 2021, **7**, 714–725.
15 Z. Ke, M. Lan, T. Yang, W. Jia, Z. Gou, K. Chen and J. Jiang, *Environ. Res.*, 2021, **198**, 111216.
16 J. Liu, X. Zhang, Y. Li, W. Li, C. Hang and V. K. Sharma, *Water Res.*, 2019, **150**, 68–76.
17 J. Gao, L. Liu, X. Liu, J. Lu, H. Hao, H. Yuan and H. Zhou, *Water Sci. Technol.*, 2012, **65**, 998–1006.
18 W. Zhong, D. Wang, X. Xu, Q. Luo, B. Wang, X. Shan and Z. Wang, *Chemosphere*, 2010, **80**, 998–1005.
19 Z. Zhang, Q. Zhu, C. Huang, M. Yang, J. Li, Y. Chen, B. Yang and X. Zhao, *Water Res.*, 2020, **170**, 115283.
20 L. Bu, X. Chen, Y. Wu and S. Zhou, *Sep. Purif. Technol.*, 2023, 123119.
21 S. D. Richardson and C. Postigo, *Advances in the Use of Liquid Chromatography Mass Spectrometry (LC-MS)—Instrumentation Developments and Applications*, 2018, pp. 267–295.
22 Y. Zhang, C. Cao, Z. Yang, G. Jia, X. Liu, X. Li, Z. Cui and A. Li, *J. Food Compos. Anal.*, 2023, **115**, 104877.
23 Y. Li, M. A. Taggart, C. McKenzie, Z. Zhang, Y. Lu, S. Pap and S. W. Gibb, *J. Environ. Sci.*, 2021, **100**, 18–27.
24 J. Zheng, H. Zhao, G. Ning, W. Sun, L. Wang, H. Liang, H. Xu, C. He, H. Zhao and C. P. Li, *Talanta*, 2021, **233**, 122520.
25 B. Rajeswari, B. Sravani, M. Cheffena, R. Janraj Naik, Y. Veera Manohara Reddy, G. Madhavi, K. V. N. Suresh Reddy and M. Jong Kim, *Inorg. Chem. Commun.*, 2023, **151**, 110627.
26 H. Liang, C. Chen, J. Zeng, M. Zhou, L. Wang, G. Ning, Q. Duan, R. Han, H. Liu, H. Zhao and C.-P. Li, *ACS Appl. Nano Mater.*, 2022, **5**, 16774–16783.
27 M. U. Anu Prathap, B. Kaur and R. Srivastava, *Chem. Rec.*, 2019, **19**, 883–907.
28 C.-S. Liu, J. Li and H. Pang, *Coord. Chem. Rev.*, 2020, **410**, 213222.
29 H. Wu, A. Li, J. Wang, X. Li, M. Cui, N. Yang, Y. Liu, L. Zhang, X. Wang and G. Zhan, *Environ. Res.*, 2022, **210**, 112985.
30 Y. Chu, X. Wang, L. Wang, Z. Chen, Y. Zhu and F. Zhao, *J. Electroanal. Chem.*, 2022, **921**, 116601.
31 X. Fang, Z. Zeng, Q. Li, Y. Liu, W. Chu, T. Maiyalagan and S. Mao, *Sens. Actuators, B*, 2021, **332**, 129526.
32 J. Zhang, S. Cui, Y. Ding, X. Yang, K. Guo and J. T. Zhao, *Biosens. Bioelectron.*, 2018, **112**, 177–185.
33 W. Meng, Y. Wen, L. Dai, Z. He and L. Wang, *Sens. Actuators, B*, 2018, **260**, 852–860.
34 H. Karimi-Maleh, H. Beitollahi, P. S. Kumar, S. Tajik, P. M. Jahani, F. Karimi, C. Karaman, Y. Vasseghian, M. Baghayeri and J. Rouhi, *Food Chem. Toxicol.*, 2022, **164**, 112961.
35 L. Qian, S. Durairaj, S. Prins and A. Chen, *Biosens. Bioelectron.*, 2021, **175**, 112836.
36 M. Wang, Y. Liu, L. Yang, K. Tian, L. He, Z. Zhang, Q. Jia, Y. Song and S. Fang, *Sens. Actuators, B*, 2019, **281**, 1063–1072.
37 M. Taran, M. Safaei, N. Karimi and A. Almasi, *Biointerface Res. Appl. Chem.*, 2021, **11**, 7860–7870.
38 R. K. Sharma, K. Solanki, R. Dixit, S. Sharma and S. Dutta, *Environ. Sci.: Water Res. Technol.*, 2021, **7**, 818–860.
39 Q. He, B. Wang, J. Liu, G. Li, Y. Long, G. Zhang and H. Liu, *Environ. Res.*, 2022, **214**, 114007.
40 S. Pal, S.-S. Yu and C.-W. Kung, *Chemosensors*, 2021, **9**, 306.
41 L. Liu, Y. Zhou, S. Liu and M. Xu, *ChemElectroChem*, 2018, **5**, 6–19.
42 N. Kajal, V. Singh, R. Gupta and S. Gautam, *Environ. Res.*, 2022, **204**, 112320.
43 C. H. Chuang and C. W. Kung, *Electroanal*, 2020, **32**, 1885–1895.
44 M. Liu, Z. Xing, Z. Li and W. Zhou, *Coord. Chem. Rev.*, 2021, **446**, 214123.
45 M.-X. Wu, Y. Wang, G. Zhou and X. Liu, *ACS Appl. Mater. Interfaces*, 2020, **12**, 54285–54305.
46 Y.-C. Wang, Y.-C. Chen, W.-S. Chuang, J.-H. Li, Y.-S. Wang, C.-H. Chuang, C.-Y. Chen and C.-W. Kung, *ACS Appl. Nano Mater.*, 2020, **3**, 9440–9448.
47 D. Sun, D. Yang, P. Wei, B. Liu, Z. Chen, L. Zhang and J. Lu, *ACS Appl. Mater. Interfaces*, 2020, **12**, 41960–41968.
48 Z. Peng, Z. Jiang, X. Huang and Y. Li, *RSC Adv.*, 2016, **6**, 13742–13748.
49 T. Liu, M. Zhou, Y. Pu, L. Liu, F. Li, M. Li and M. Zhang, *Sens. Actuators, B*, 2021, **342**, 130047.
50 J. Li, M. Liu, Y. Li, L. Yuan, P. Zhang, Z. Cai, H. Chen and J. Zou, *Mater. Today Energy*, 2021, **19**, 100574.

51 A. T. Gu, J. Y. Chen, Q. H. Gao, M. M. Khan, P. Wang, Y. Jiao, Z. X. Zhang, Y. Liu and Y. Yang, *Appl. Surf. Sci.*, 2020, **516**, 14160.
52 A. Aijaz, A. Karkamkar, Y. J. Choi, N. Tsumori, E. Ronnebro, T. Autrey, H. Shioyama and Q. Xu, *J. Am. Chem. Soc.*, 2012, **134**, 13926–13929.
53 Y. Wang, Y. Wang, L. Zhang, C.-S. Liu and H. Pang, *Inorg. Chem. Front.*, 2019, **6**, 2514–2520.
54 B. Zheng, M. Sant, P. Demontis and G. B. Suffritti, *J. Phys. Chem. C*, 2012, **116**, 933–938.
55 Y. Li, Z. Jin and T. Zhao, *Chem. Eng. J.*, 2020, **382**, 123051.
56 Z. Huang, J. Zhou, Y. Zhao, H. Cheng, G. Lu, A. W. Morawski and Y. Yu, *J. Mater. Res.*, 2021, **36**, 602–614.
57 T. L. H. Doan, J.-Y. Kim, J.-H. Lee, L. H. T. Nguyen, Y. T. Dang, K.-B. T. Bui, A. T. T. Pham, A. Mirzaei, T. B. Phan and S. S. Kim, *Sens. Actuators, B*, 2021, **348**, 130648.
58 R. Huang, D. Liao, Z. Liu, J. Yu and X. Jiang, *Sens. Actuators, B*, 2021, **338**, 129828.
59 H. Yang, S. Li, H. Yu, F. Zheng, L. Lin, J. Chen, Y. Li and Y. Lin, *Nanoscale*, 2019, **11**, 8950–8958.
60 U. Solaem Akond, K. Barman, A. Mahanta and S. Jasimuddin, *Electroanal*, 2020, **33**, 900–908.
61 N. Manjula and S.-M. Chen, *Microchem. J.*, 2021, **168**, 106514.
62 U. Chakraborty, G. Bhanjana, N. Kannu, N. Kaur, R. Sharma, G. Kaur, A. Kaushik and G. R. Chaudhary, *J. Hazard. Mater.*, 2021, **416**, 125771.
63 V. Anbumannan, M. Dinesh, R. T. Rajendra Kumar and K. Suresh, *Ceram. Int.*, 2019, **45**, 23097–23103.